This article is published as part of the *Dalton Transactions* themed issue entitled:

Computational Chemistry of Molecular Inorganic Systems

Guest Editor: Professor Stuart MacGregor
Heriot-Watt University, Edinburgh, U.K.

Published in issue 42, 2011 of *Dalton Transactions*

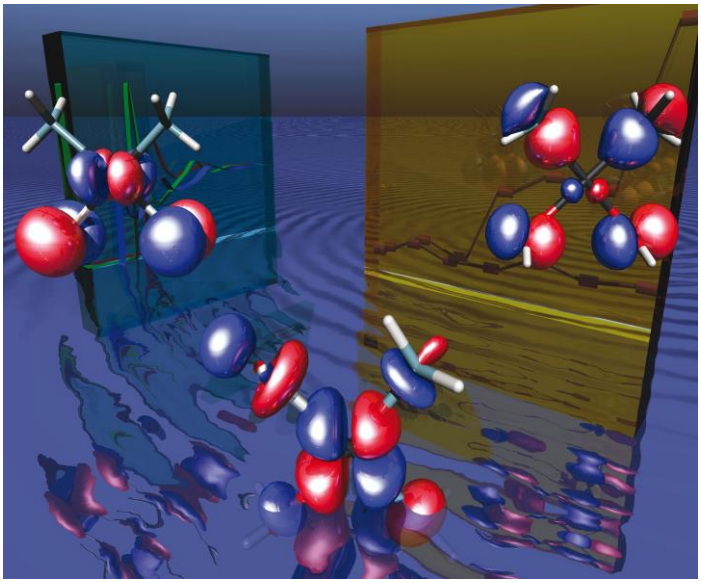

Image reproduced with the permission of Hirofumi Sato

Articles in the issue include:

COMMUNICATION:
Comparison of different ruthenium–alkylidene bonds in the activation step with N-heterocyclic carbene Ru-catalysts for olefins metathesis
Albert Poater, Francesco Ragone, Andrea Correa and Luigi Cavallo
Dalton Trans., 2011, DOI: 10.1039/C1DT10959F

HOT ARTICLES:
Matrix infrared spectroscopic and density functional theoretical investigations on thorium and uranium atom reactions with dimethyl ether
Yu Gong and Lester Andrews
Dalton Trans., 2011, DOI: 10.1039/C1DT10725A

Reductive coupling of carbon monoxide by U(III) complexes—a computational study
Georgina Aitken, Nilay Hazari, Alistair S. P. Frey, F. Geoffrey N. Cloke, O. Summerscales and Jennifer C. Green
Dalton Trans., 2011, DOI: 10.1039/C1DT10692A

Prediction of high-valent iron K-edge absorption spectra by time-dependent Density Functional Theory
P. Chandrasekaran, S. Chantal E. Stieber, Terrence J. Collins, Lawrence Que, Jr., Frank Neese and Serena DeBeer
Dalton Trans., 2011, DOI: 10.1039/C1DT11331C

Visit the *Dalton Transactions* website for more cutting-edge inorganic and organometallic research
www.rsc.org/dalton

Dalton Transactions

Dynamic Article Links

Cite this: *Dalton Trans.*, 2011, **40**, 11115

www.rsc.org/dalton

PAPER

Infrared spectra of CH_3–MH, CH_3–M, and CH_3–MH^- prepared *via* methane activation by laser-ablated Au, Ag, and Cu atoms†

Han-Gook Cho[a] and Lester Andrews*[b]

Received 24th December 2010, Accepted 24th February 2011
DOI: 10.1039/c0dt01827a

Methane activation by laser-ablated, excited Group 11 metal atoms has been carried out, leading to generation of CH_3–MH, CH_3–M, and CH_3–MH^-, which are identified in the product infrared spectra on the basis of isotopic shifts and correlation with DFT calculated frequencies. The products reveal that C–H insertion by excited Au, Ag, and Cu readily occurs, and subsequent hydride-detachment or electron addition also follows. Each type of product has similar photochemical properties regardless of the metal. DFT computed energies reveal facile hydride dissociation and high electron affinities for the insertion complexes. The methyl metal species have the shortest C–M bonds, consistent with their highest calculated effective bond order, and the CH_3–MH complexes have higher electron affinities than the metal atoms.

Introduction

Group 11 metals have played distinctive roles for making coinage, jewelry, and art since the beginning of human history. They are at the borderline between the main group elements and transition-metals due to their d^{10} electronic configuration.[1–3] The coinage metals often behave as Lewis acids with their relatively large electron affinities. In particular, gold has a small atomic radius and the highest electronegativity (2.54) among transition-metals along with its strong relativistic contraction, and its chemistry has been investigated extensively.[1] Recently there has been an upsurge of research activity in homo- and heterogeneous catalytic reactions by the coinage metals, which provide detailed information on their complexes, particularly with π systems.[1–3]

Coinage metal complexes with carbon–metal bonds are rare. Alkyl silver was first prepared by reaction of tetra-alkyl lead and silver nitrate at liquid nitrogen temperature,[4] and alkyl copper by reaction of alkyl lithium and cuprous chloride below 0° C.[5] Grotjahn *et al.* characterized CH_3–Cu with gas phase rotational spectra.[5a] Parnis *et al.* reported the formation of CuH, CH_3–CuH, and CH_3–Cu in a CH_4 matrix after UV irradiation, and provided clear evidence that the reaction proceeds with Cu excited to the ^2P state,[6a] which is in line with the later finding of the Weisshaar group that ground state copper atoms are not reactive with alkanes in the gas phase.[6c] Chang *et al.* observed $CuCH_2$ in the matrix IR spectra from the reaction of Cu with CH_2N_2.[7] Rijs and O'Hair have observed anionic Ag and Cu insertion complexes (CH_3–AgH^- and CH_3–CuH^-) and dialkyl metals in the fragmentation of $[RCO_2AgO_2CR]^-$ by means of mass spectrometry.[8]

Extensive recent studies have shown that C–H activation of alkanes by transition-metal atoms is in fact a general phenomenon, leading to small insertion and high oxidation-state complexes (carbenes and carbynes).[9–13] Their small sizes are amenable to high-level computations,[14] and many of them show interesting structural distortions and photochemical reactions. In this study, we report the results of Group 11 metal atom reactions with methane in excess argon. The products are identified on the basis of isotopic shifts and correlation with DFT calculations. Thus, coinage metal atoms are also effective methane activation agents.

Experimental and computational methods

Laser ablated Au, Ag, and Cu atoms were reacted with CH_4 (Matheson, UHP grade), $^{13}CH_4$, CD_4, CH_2D_2 (Cambridge Isotopic Laboratories) in excess argon during condensation at 8 K using a closed-cycle refrigerator (Air Products Displex). Reagent gas mixtures ranged 0.5–5.0% (typically 2%) in argon. A small amount of CCl_4 (Fisher) was added to the sample (~0.02%) as an electron scavenger in selected experiments to gain information for the identification of ionic species as described in previous publications.[9,15] The Nd : YAG laser fundamental radiation (1064 nm, 10 Hz repetition rate, 10 ns pulse width) was focused on rotating Au, Ag, and Cu targets using 5–10 mJ $pulse^{-1}$, and the ablated material was co-deposited with the argon–methane samples as illustrated.[9] After initial reaction, infrared spectra were recorded at 0.5 cm^{-1} resolution using a Nicolet 550 spectrometer with a Hg–Cd–Te range B detector. Then samples were irradiated for 20 min periods by a mercury arc street lamp (175 W) with the globe removed using a combination of optical filters and were annealed to allow further reagent diffusion.

[a]*Department of Chemistry, University of Incheon, 12-1 Songdo-dong, Yonsu-gu, Incheon, 406-772, South Korea*
[b]*Department of Chemistry, University of Virginia, P. O. Box 400319, Charlottesville, Virginia, 22904-4319. E-mail: lsa@virginia.edu*
† Electronic supplementary information (ESI) available. See DOI: 10.1039/c0dt01827a

To provide support for the assignment of new experimental frequencies and to correlate with related work,[9–13] density functional theory (DFT) calculations were performed using the Gaussian 09 program system,[16] the B3LYP density functional,[17] the 6-311++G(3df,3pd) basis sets for H, C, and Cu[18] and SDD core potential and basis sets for Au and Ag[19] to provide vibrational frequencies for the reaction products. Geometries were fully relaxed during optimization, and the optimized geometry was confirmed by vibrational analysis. The BPW91[20] functional and MP2[21] method were also employed to complement the B3LYP results. The vibrational frequencies are calculated analytically, and zero-point energy is included in the calculation of binding and reaction energies. Previous investigations have shown that DFT calculated harmonic frequencies are usually slightly higher than observed frequencies,[9–13,22,23] and they provide useful predictions for the infrared spectra of new molecules.

Results and discussion

The matrix infrared spectra (Fig. 1–6 and S1–3†, and Table 1–3) from reactions of laser-ablated Au, Ag, and Cu atoms with methane isotopomers were investigated, and DFT frequency calculations of the products (Tables S1–S9†) and their structures (Fig. 7–9) will be presented in turn.

Au + CH_4

Infrared spectra are shown in Fig. 1 for the reaction products of laser ablated Au atoms co-deposited with CH_4 and with CH_4 + CCl_4 in excess argon during condensation at 8 K. Fig. 2 and S1† show the corresponding absorptions from the deuterated and half deuterated products. Three groups of product absorptions are observed (marked "**i**, **a**, and **i**$^-$" for insertion, methyl auride, and insertion product anion). The absorption groups are based on the intensity variations upon photolysis and annealing. The **i** absorptions vanish on visible ($\lambda > 420$ nm) irradiation, but reappear on UV ($240 < \lambda < 380$ nm) irradiation and further increase on full arc ($\lambda > 220$ nm) irradiation and annealing to ~50% of the original intensity. The **a** absorptions increase by ~5, ~25, and ~10% on visible, UV, and full arc photolysis (~40% increase in total) and decrease markedly on annealing. The **i**$^-$ absorptions remain almost unchanged on visible irradiation, but decrease ~30% each on UV and full arc irradiation.

Table 1 Observed frequencies and assignments for the product absorptions from Au + methane isotopomer reactions[a]

Group[b]	CH_4	CD_4	$^{13}CH_4$	CH_2D_2	Description[c]
i	1853.5				CH_3–AuH, Au–H stretch
	1044.9	790.3	1040.2	977.0, 898.4	CH_3–AuH, CH_3 deform
				644.0	CH_3–AuH, CH_3 rock
a	1188.3, **1181.7**	925.7, **920.5**	1178.4, **1173.3**	1123.6, **983.2**	CH_3Au, CH_3 deform
	794.5	584.0	790.6	784.4, 599.7, 697.7	CH_3Au, CH_3 rock
i$^-$	1868.7	1341.5	1868.7	1866.6, 1345.7	CH_3–AuH$^-$, Au–H stretch
		858.0			CH_3–AuH$^-$, CH_3 deform
	726.6	553.4	722.8		CH_3–AuH$^-$, CH_3 rock

[a] Observed in an argon matrix. Frequencies are in cm^{-1}. [b] Product absorption group on the basis of intensity variation in the process of photolysis and annealing. [c] Designated product and vibrational mode.

Table 2 Observed frequencies and assignments for the product absorptions from Ag + methane isotopomer reactions[a]

Group[b]	CH_4	CD_4	$^{13}CH_4$	CH_2D_2	Description[c]
a	1076.4	824.1	1069.3	917.1	CH_3–Ag, CH_3 deform
	666.1	499.1	663.6	586.7	CH_3–Ag, CH_3 rock
i$^-$	1562.0	1124.2	1562.0	1560.9	CH_3–AgH$^-$, Ag–H stretch

[a] Observed in an argon matrix. Frequencies are in cm^{-1}. [b] Product absorption group on the basis of intensity variation in the process of photolysis and annealing. [c] Designated product and vibrational mode.

Table 3 Observed frequencies and assignments for the product absorptions from Cu + methane isotopomer reactions[a]

Group[b]	CH_4	CD_4	$^{13}CH_4$	CH_2D_2	Description[c]
CuH	1878.5 (1850)[d]	1353.9 (1333)	1879.1 (1850)	1878.7, 1353.9	CuH, Cu–H stretch
i	1718.8 (1697)[d]	1243.7 (1229)	1717.7 (1697)	1718.9, covered	CH_3–CuH, Cu–H stretch
	1012.1 (1011)[d]	786.0 (786)	1003.6 (1003)	861.0	CH_3–CuH, CH_3 deform
a	1203.0 (1196)[d]	920.0 (916)	1195.1 (1189)		CH_3–Cu, CH_3 deform
	648.3	494.2	645	637.2, 594.4, 563.7, 498.1	CH_3–Cu, CH_3 rock
i$^-$	1612.9	1165.0	1612.9	1611.9, 1166.0	CH_3–CuH$^-$, Cu–H stretching

[a] Observed in an argon matrix. Frequencies are in cm^{-1}. [b] Product absorption group on the basis of intensity variation in the process of photolysis and annealing. [c] Designated product and vibrational mode. [d] Observed in solid methane matrix, ref. 6a.

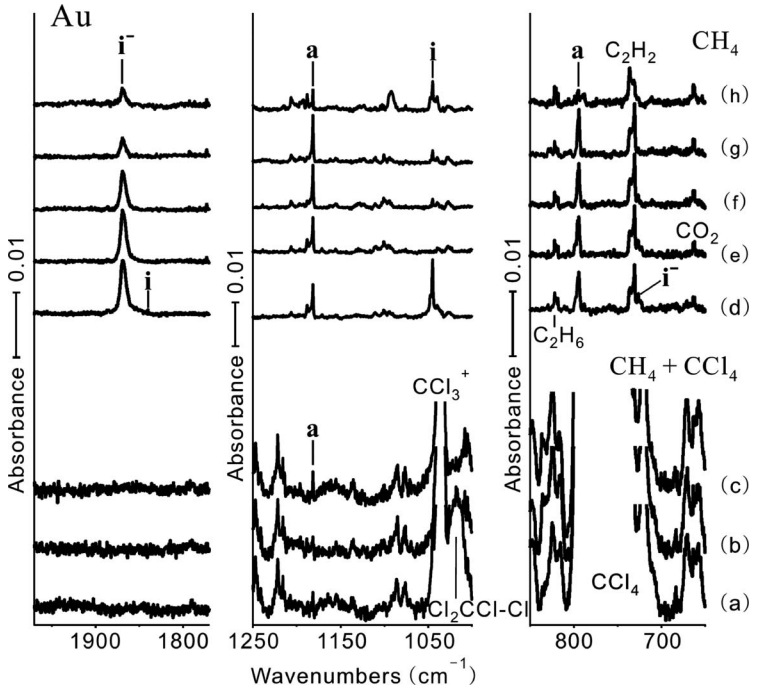

Fig. 1 Infrared spectra in the 1970–1770, 1250–1000, and 850–650 cm^{-1} regions for the reaction products of the laser-ablated gold atom with CH_4 and with CH_4 + CCl_4 in excess argon at 8 K. (a) Au and CH_4 + CCl_4 (2.0 and 0.02% in argon) co-deposited for 1 h, (b) as (a) after visible (λ > 420 nm) irradiation, and (c) as (b) after UV (240–380 nm) irradiation. (d) Au and CH_4 reagent (2.0% in argon) co-deposited for 1 h, (e)–(g) as (d) after visible, UV, and full arc (λ > 220 nm) irradiation, and (h) as (g) after annealing to 26 K. **a**, **i**, and **i**$^-$ stand for product absorption groups. Common products from CCl_4, which was added to serve as an electron scavenger in the matrix sample, are labelled.

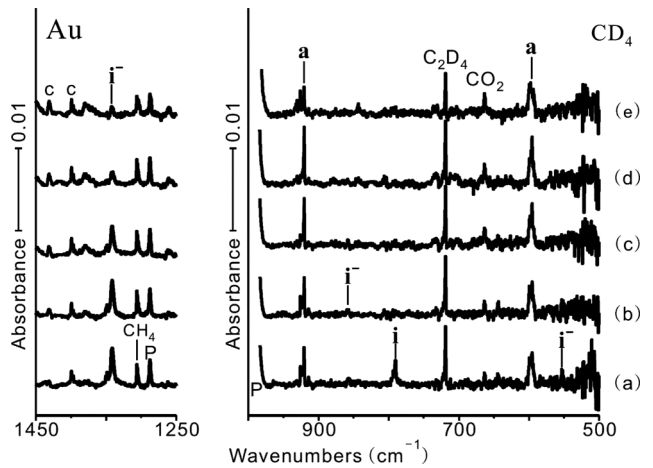

Fig. 2 Infrared spectra in the 1450–1250 and 1000–500 cm^{-1} regions for the reaction products of the laser-ablated gold atom with CD_4 in excess argon at 8 K. (a) Au and CD_4 (2.0% in argon) co-deposited for 1 h, (b)–(d) as (a) after visible, UV, and full arc irradiation, and (e) as (d) after annealing to 26 K. **a**, **i**, and **i**$^-$ stand for product absorption groups while P and c stand for the precursor and common absorptions from methane.

A strong **i** absorption observed at 1044.9 cm^{-1} has its D and ^{13}C counterparts at 790.3 and 1040.2 cm^{-1} (H : D and 12 : 13 ratios of 1.322 and 1.005). Absorptions from partly deuterated products are also observed at 977.0 and 898.4 cm^{-1} in the CH_2D_2 spectra in Fig. S1.† The strong absorption showing large D and small C shifts is assigned to the CH_3 deformation mode of the most probable insertion complex (CH_3–AuH). The observed frequency and D and ^{13}C isotopic shifts (254.6 and 4.7 cm^{-1}) are compared with the B3LYP values of 1089.7, 264.6, and 5.5 cm^{-1} for the strongest absorption. The observed product frequencies in the CH_2D_2 spectra are also in line with the B3LYP values of 1018.4 and 922.7 cm^{-1} for CH_2D–AuD and CHD_2–AuH.

The weak **i** absorptions observed at 1853.5 and 644.0 cm^{-1} in the CH_4 and CH_2D_2 spectra are assigned to the Au–H stretching and CH_3 rocking modes as shown in Table 1. The excellent agreement between the observed and computed frequencies and isotopic shifts substantiates formation of the gold insertion complex (CH_3–AuH) in the doublet ground state (Table S1†). The present results show that the ordinarily unreactive gold atom, upon excitation, undergoes C–H insertion with CH_4, producing a simple insertion complex like other transition-metals (Groups 3–10), lanthanides, and actinides.[9–13] This reaffirms that C–H insertion by an excited transition-metal is a general chemical phenomenon.

The **a** absorption at 1181.7 cm^{-1} shows D and ^{13}C counterparts at 920.5 and 1173.3 cm^{-1} (H : D and 12 : 13 ratios of 1.284 and 1.007, respectively). We assign this absorption to the CH_3 deformation mode of methyl auride (CH_3–Au) on the basis of the good agreement with the predicted values (*e.g.* B3LYP values of 1199.5, 922.2, and 1192.2 cm^{-1} for CH_3–Au, CD_3–Au, and $^{13}CH_3$–Au shown in Table S2†). The observed frequencies of 1123.6 and 983.2 cm^{-1} in the CH_2D_2 spectra are also consistent with the B3LYP values of 1125.6 and 999.0 cm^{-1} for CH_2D–Au and CHD_2–Au.

The stronger **a** absorption at 794.5 cm^{-1} carries D and ^{13}C counterparts at 584.0 and 790.6 cm^{-1}, (compared with the B3LYP values of 803.4, 594.0, and 799.9 cm^{-1}) and it is assigned to the CH_3 rocking mode of methyl auride. The observed frequencies of 784.4, 697.7, and 599.7 cm^{-1} in the CH_2D_2 spectra are in

line with the predicted values of 790.3 cm^{-1} for CH_2D–Au and 697.5 and 596.4 cm^{-1} for CHD_2–Au. The observed frequencies, isotopic shifts, and good agreement with the predicted values all provide strong evidence for formation of another primary product of methane activation by gold, CH_3–Au.

Because the auride anion lies between bromide and iodide in size,[1g] it may be interesting to compare some properties of CH_3I and CH_3Au. The B3LYP Mulliken charges for CH_3Au (–0.54, 0.07 × 3 and 0.32) are similar to those of CH_3I (–0.44, 0.10 × 3 and 0.14), but the dipole moment 0.20 D is smaller than that of CH_3I, 1.75 D. Likewise the methyl deformation frequencies are also similar 1181.7 and 794.5 cm^{-1} for CH_3Au, and 1245 and 882 cm^{-1} for CH_3I in solid argon.

The strongest product absorption in the original deposition spectra in Fig. 1 is observed at 1868.7 cm^{-1} (marked "**i**$^-$"), its D counterpart is observed at 1341.5 cm^{-1} (H : D ratio of 1.393), and it reveals a negligible ^{13}C shift, as shown in Table 1 and S3.† The frequency is also compared with the previously reported Au–H stretching frequencies of 2082, 1991.7, 1676.4, 1661.5, and 1636.0 cm^{-1} for AuAuH, $AuAuH^-$, AuH_4^-, $(H_2)AuH_3$, and AuH_2^-,[24] which are not observed in this study. This strong **i**$^-$ absorption not only decreases on UV and full arc ($240 < \lambda < 380$ nm and $\lambda > 220$ nm) irradiation, but also disappears from the product spectrum when trace CCl_4 is added to the reagent mixture as shown in Fig. 1. Extensive work in this laboratory has demonstrated that CCl_4 is an effective electron scavenger in matrix samples,[15,24] and this chemical diagnostic facilitates the identification of anion product absorptions. Isolated anions have been observed in previous laser ablation matrix isolation experiments owing to the production of electrons in the ablation process.[15,24] We assign the **i**$^-$ absorption to the Au–H stretching mode of the methyl gold hydride anion (CH_3–AuH^-), the most probable anionic insertion complex.

Its frequency and high absorption intensity are also well reproduced by electronic structure computations for the singlet ground state; however, the DFT and MP2 results differ somewhat as the latter tends to over estimate frequencies. For example, the B3LYP and MP2 Au–H stretching frequencies are 1843.7 and 1992.2 cm^{-1}. In addition the MP2 computation gives a C_{3v} structure similar to the previously studied Ag and Cu analogues[8] while the DFT methods give a near C_{3v} structure. The distinctively very strong Au–H stretching absorption of CH_3–AuH^- is in contrast to the weak counterpart for CH_3–AuH. A weak possible **i**$^-$ absorption at 726.6 cm^{-1} shifts to 553.4 and 722.8 cm^{-1} on deuteration and ^{13}C substitution. The frequency, large D and small ^{13}C shifts, and correlation with computational results allow tentative assignment of this as the CH_3 rocking mode (Table 1 and S3†). The triplet state is 241 kJ mol^{-1} higher in energy, and the strong Au–H stretching mode predicted near 1530 cm^{-1} is not observed. The observed frequencies and isotopic shifts and the agreement with the predicted values for the singlet ground state all support formation of the anionic gold insertion complex with a very intense infrared absorbing Au–H stretching mode.

Other plausible anionic species with an Au–H bond, such as CH_2–AuH^-, were also examined computationally, but the predicted vibrational characteristics (strong absorptions at 1863 and 602 cm^{-1} for CH_2–AuH^- and at 1765 cm^{-1} for CH–AuH^-) are not consistent with the observed values. The high electron affinity of gold is profound, the largest (–223 kJ mol^{-1}) in the periodic table with the exception of the halogens.[1g,25] Various anionic gold complexes have been reported,[26] and more recently anionic Group 11 metal hydrides are also identified in the matrix spectra from reactions of laser ablated Au and electrons with H_2.[24] The formation of an anionic species in the reaction of Au with CH_4 is, therefore, not surprising.

CH_3–AuH, CH_3–Au, and CH_3–AuH^- are 80, –211, and 26 kJ mol^{-1} higher in energy than Au(^{2}S) + CH_4, Au(^{2}S) + CH_3, and Au^-(^{1}S) + CH_4, respectively. However, the insertion reaction probably proceeds *via* Au(^{2}P), which is 446 kJ mol^{-1} higher in energy than Au(^{2}S),[27] so the insertion product is 367 kJ mol^{-1} lower in energy than Au(^{2}P) + CH_4 reagents. Nevertheless, the identified products are the most stable among the plausible products. For example, the unidentified CH_2–AuH_2, CH_2–AuH, and CH_2–AuH_2^- are 157, 5.6, and 340 kJ mol^{-1} higher than the corresponding reference energies (Au(^{2}S) + CH_4, Au(^{2}S) + CH_3, and Au^-(^{1}S) + CH_4). The high energy of CH_3–AuH is in line with the disappearance of the **i** absorptions on visible irradiation, whereas during UV and full arc photolysis the **i** and **a** absorptions increase owing to $^2P \Leftarrow {}^2S$ excitation of Au,[27] while the **i**$^-$ absorptions decrease as shown in Fig. 1, 2, and S1,† raising the possibility that UV irradiation causes detachment of an electron from CH_3–AuH^-.

CH_3 is also produced by the laser plume radiation during co-deposition of Au and CH_4, leaving the broad CH_3 absorption at 620–600 cm^{-1}, parallel to the previously studied reactions of laser ablated transition-metal atoms with methane.[9–13] Milligan and Jacox showed that 121.6 nm radiation is effective for dissociation of the C–H bond during deposition of CH_4 to generate the CH_3 radical.[28] However, the concentration of CH_3 is still very low relative to that of CH_4, and in our previously studied reactions of transition-metals with methane, methyl metal species have not been identified.[9–13] The ablation plume also contains electrons, providing opportunity for anionic species to form, but anionic species have only been observed in methane activation by transition-metals in the case of the Nb and Ta methylidyne anions.[9–13]

Ag + CH_4

The product absorptions marked "**a**" and "**i**$^-$" from Ag reactions with CH_4 and CH_4 + CCl_4 in Fig. 3 show intensity variations similar to those of the Au counterparts on photolysis and annealing. They remain unchanged on visible irradiation, but the **a** absorptions increase on UV and full arc photolysis while the **i**$^-$ absorptions decrease. They are weaker than in the Au + CH_4 case and no **i** absorptions are observed.

The **a** absorption at 1076.4 cm^{-1} is accompanied by D and ^{13}C counterparts at 824.1 and 1069.3 cm^{-1} (H/D and 12/13 ratios of 1.306 and 1.007) (Fig. 4), and the frequency, large D and small ^{13}C shifts, and consistency with the Au case lead to their assignment to the CH_3 deformation mode of methyl silver (CH_3–Ag), which is the second strongest band of the product. The observed frequencies of the CH_3–Ag isotopomers are in good correlation with the B3LYP values of 1097.7, 845.4, and 1090.6 cm^{-1} (Table S5†). The **a** absorption observed at 917.1 cm^{-1} in the CH_2D_2 spectra is in line with the calculated value of 931.0 cm^{-1} for CHD_2–Ag. Another **a** absorption is observed at 666.1 cm^{-1} with D and ^{13}C counterparts at 499.1 and 663.6 cm^{-1} (H : D and 12 : 13 ratios of 1.335 and

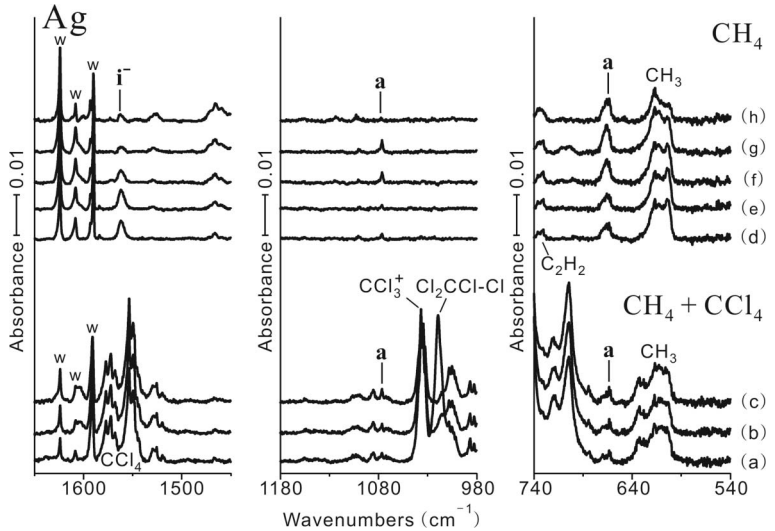

Fig. 3 Infrared spectra in the 1650–1450, 1180–980, and 740–540 cm^{-1} regions for the reaction products of the laser-ablated silver atom with CH_4 and $CH_4 + CCl_4$ in excess argon at 8 K. (a) Ag and $CH_4 + CCl_4$ (2.0 and 0.02% in argon) co-deposited for 1 h, (b) and (c) as (a) after visible and UV irradiation. (d) Ag and CH_4 reagent (2.0% in argon) co-deposited for 1 h, (e)–(g) as (d) after visible, UV, and full arc irradiation, (h) as (g) after annealing to 26 K. **a** and $\mathbf{i}^-$ stand for product absorption groups while w designates water residue absorptions.

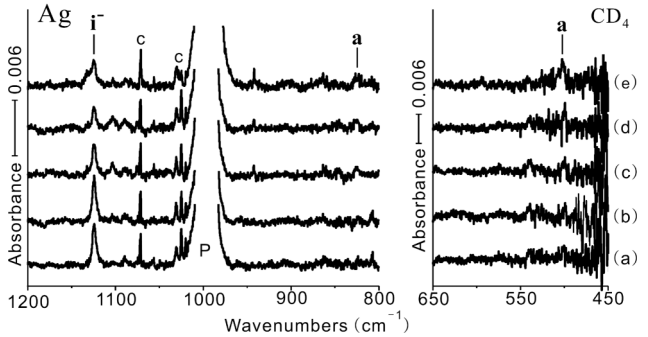

Fig. 4 Infrared spectra in the 1200–800 and 650–450 cm^{-1} regions for the reaction products of the laser-ablated silver atom with CD_4 in excess argon at 8 K. (a) Ag and CD_4 (2.0% in argon) co-deposited for 1 h, (b)–(d) as (a) after visible, UV, and full arc irradiation, and (e) as (d) after annealing to 26 K. **a** and $\mathbf{i}^-$ stand for product absorption groups while P and c stand for the precursor and common absorptions.

1.004), and we assign it to the strongest mode, CH_3 rocking. The observed frequencies are again in an excellent agreement with the DFT values (*e.g.* B3LYP values of 693.6, 512.7, and 690.7 cm^{-1}), and the observed frequency of 586.7 cm^{-1} in the CH_2D_2 spectra correlates with the predicted value of 604.6 cm^{-1} for CHD_2–Ag, substantiating formation of CH_3–Ag.

The $\mathbf{i}^-$ absorption at 1562.0 cm^{-1} has its D counterpart at 1124.2 cm^{-1} (H : D ratio of 1.389), but shows no ^{13}C shift. This Ag–H stretching frequency is compared with those at 1746.5, 1717.0, 1691.9, and 1427.5 cm^{-1} found for $(H_2)AgH$, AgH, AgAgH, and AgH_2^-,[24] which are not observed in this study. The $\mathbf{i}^-$ Ag–H stretching absorption also disappears on addition of CCl_4 and it is accordingly assigned to CH_3–AgH^-. Its frequency and high absorption intensity are in reasonable agreement with the B3LYP and BPW91 computed frequencies of 1554.6 and 1575.5 cm^{-1} and large intensities of 615 and 587 km mol^{-1} (Table S6†). The triplet state is 223 kJ mol^{-1} higher in energy, and the strong Ag–H stretching mode predicted near 1280 cm^{-1} is not observed. The observed frequencies and isotopic shifts and the agreement with the predicted values for the singlet ground state all support this assignment.

Rijs and O'Hair have shown that CH_3–AgH^- and CH_3–CuH^- are among the primary products in gas phase fragmentation reactions of $[RCO_2MO_2CR]^-$.[8] They examined the reaction paths by DFT calculations and collision-induced dissociation and deuterium labeling experiments, and showed that a diverse set of pathways including bond homolysis, bond heterolysis, and β-hydride elimination were apparently involved. The present results reveal that a combination of laser ablation and direct reaction with alkanes is an effective method to provide the anionic coinage metal insertion complexes.

As in the Au case, CH_3–AgH, CH_3–Ag, and CH_3–AgH^- are 161, −154, and 43 kJ mol^{-1} higher than $Ag(^2S) + CH_4$, $Ag(^2S) + CH_3$, and $Ag^-(^1S) + CH_4$, respectively. The higher energies of the products relative to those in the Au case are consistent with the weaker product absorptions. In particular, the endothermicity of 161 kJ mol^{-1} for CH_3–AgH is much higher than the value of 80 kJ mol^{-1} for CH_3–AuH, providing some rationale for the absence of its absorptions. However, the anion is most likely produced by electron capture of this neutral molecule, but note that the infrared intensity of the anion Ag–H vibration is on the order of 40 times larger than for the neutral analogue. Using the $Ag(^2P)$ reagent, the reaction to form CH_3–AgH is 192 kJ mol^{-1} exothermic. Other plausible products are still energetically even higher. For example, CH_2–AgH_2, CH_2–AgH, and CH_2–AgH_2^- are 235, 125, and 373 kJ mol^{-1} higher than the corresponding references.

Cu + CH_4

Fig. 5 shows the reaction product spectra from Cu atoms co-deposited with CH_4 and with $CH_4 + CCl_4$ in excess argon during condensation at 8 K. Fig. 6 and S3† show the corresponding

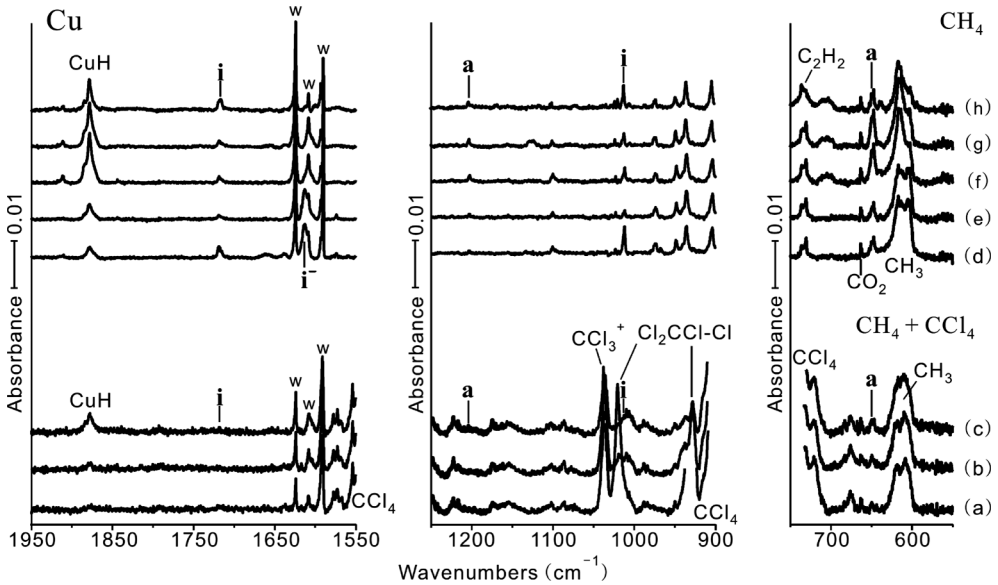

Fig. 5 Infrared spectra in the 1950–1550, 1250–900, and 750–550 cm^{-1} regions for the reaction products of the laser-ablated copper atom with CH_4 and $CH_4 + CCl_4$ in excess argon at 8 K. (a) Cu and $CH_4 + CCl_4$ (2.0 and 0.02% in argon) co-deposited for 1 h, (b) and (c) as (a) after visible and UV irradiation. (d) Cu and CH_4 reagent (2.0% in argon) co-deposited for 1 h, (e)–(g) as (d) after visible, UV, and full arc irradiation, (h) as (g) after annealing to 26 K. **a**, **i**, and **i**$^-$ stand for product absorption groups while w designates water residue absorptions.

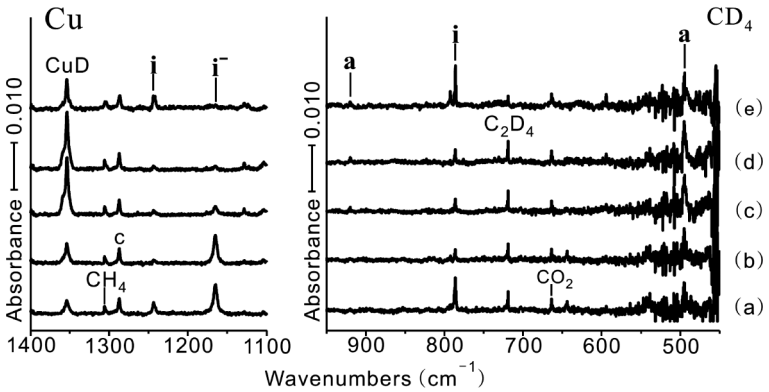

Fig. 6 Infrared spectra in the 1400–1100 and 950–450 cm^{-1} regions for the reaction products of the laser-ablated copper atom with CD_4 in excess argon at 8 K. (a) Cu and CD_4 (2.0% in argon) co-deposited for 1 h, (b)–(d) as (a) after visible, UV, and full arc irradiation, and (e) as (d) after annealing to 26 K. **a**, **i**, and **i**$^-$ stand for product absorption groups.

absorptions from the deuterated and half deuterated products. In a parallel manner to Au, three groups of product absorptions are marked "**i**, **a**, and **i**$^-$" depending on the intensity variation in the process of photolysis and annealing. The absorption intensity variation of the **i**, **a**, and **i**$^-$ absorptions are similar to those in the Au and Ag experiments.

Fig. 5 and 6 also show strong CuH and CuD absorptions at 1878.5 and 1353.9 cm^{-1} (H : D ratio of 1.387),[24] which increase slightly on visible irradiation, but more than triple on UV irradiation and slightly decrease on full arc photolysis. The strong CuH absorption contrasts with the absence of the AuH and AgH absorptions. Parnis *et al.* reported the dramatic increase of the CuH absorption at 1850 cm^{-1} along with the emergence of CH_3Cu and CH_3CuH absorptions in the methane matrix on UV (305–325 nm) irradiation.[6a]

Billups *et al.* reported the results of transition metal atom reactions in solid methane after UV irradiation, including Au, Ag, and Cu, which were assigned to the CH_3MH species.[6b] Unfortunately, these assignments are not correct: the highest frequencies reported, after calibration, are probably due to the diatomic MH molecules in solid methane.

The **i** absorption for Cu at 1718.8 cm^{-1} shifts to 1243.7 cm^{-1} on deuteration (H : D ratio = 1.382) and shows a negligible ^{13}C shift. This Cu–H stretching frequency is compared with 1862.5 and 1497.2 cm^{-1} for $(H_2)CuH$ and CuH_2^-,[24] which are observed in this study. The new Cu–H stretching absorption is assigned to CH_3–CuH, following the Au case. The observed Cu–H and Cu–D stretching frequencies and relatively low intensities are reproduced by DFT computations (*e.g.* B3LYP frequency and intensity of 1707.5 cm^{-1} and 18 km mol^{-1}, Table S7†). A stronger **i** absorption is observed at 1012.1 cm^{-1}, and its D and ^{13}C counterparts at 786.0 and 1003.6 cm^{-1} (H : D and 12 : 13 ratios of 1.288 and 1.008), and it is assigned to the CH_3 deformation mode. Again the observed frequencies are in line with the DFT frequencies (*e.g.*

the B3LYP values of 1050.3, 810.8, and 1003.6 cm^{-1}). The observed **i** absorptions correspond with the weak absorptions emerging at 1697 and 1011 cm^{-1} on UV irradiation in a solid methane matrix.[6a]

Two **a** absorptions are observed in Fig. 5. The band at 1203.0 cm^{-1} shifts to 920.0 cm^{-1} on deuteration (H : D ratio of 1.308), whereas its ^{13}C counterpart is at 1195.1 cm^{-1}. The other absorption at 648.3 cm^{-1} is much stronger and its D and ^{13}C counterparts are at 494.2 and 645 cm^{-1} (H : D and 12 : 13 ratios of 1.312 and 1.005). They are assigned to the CH_3 deformation and rocking modes of CH_3–Cu (the two strongest bands for methyl copper) on the basis of the frequencies, large D and small ^{13}C shifts, and correlation with the DFT values (Table S8†). For example the observed methyl rocking frequencies are compared with slightly higher B3LYP isotopic values of 662.7, 494.0, and 659.5 cm^{-1}. In contrast the methyl deformation frequencies are somewhat higher than the computed values. This may be due to overestimation of the C–Cu bond length (1.918 Å) in our calculation, as compared to the experimental measurement (1.8841 Å),[5a] with corresponding underestimation of the H-to-Cu repulsion, which affects the methyl deformation frequency.

Parnis *et al.* have reported eight absorption frequencies for CH_3–Cu with their D and ^{13}C counterparts,[6a] which are more than the number of vibrational modes of methyl copper (6 modes and three of them are very weak). Their 1196 cm^{-1} band and its isotopic counterparts correspond to our 1203.0 cm^{-1} absorption. In addition, these workers observed a band near 640 cm^{-1} labelled CH_3, which tracks the 1196 cm^{-1} band on irradiation, and we believe that this band should be reassigned to CH_3Cu in solid methane. The other observed frequencies do not agree with the frequencies predicted for the methyl copper (Table S8†), and thus, they probably originate from other unknown species. Recently Grotjahn *et al.* produced CH_3–Cu, the most studied coinage alkyl metal and determined the rotational constants in the ground (v = 0) and lowest excited state of the C–Cu stretch (v_3 = 1).[5a] They determined the C–Cu bond length to be 1.8841 Å and the C–Cu stretching mode to be near 586 cm^{-1}, slightly higher than our calculated value.

An **i**$^-$ absorption, which is the strongest product absorption in the original deposition spectrum, is also observed at 1612.9 cm^{-1}. Deuteration shifts it to 1165.0 cm^{-1} (H : D ratio of 1.384), and it shows no ^{13}C shift. Parallel to the Au and Ag cases, this absorption disappears on addition of CCl_4 (Fig. 5). We, therefore, assign it to the Cu–H stretching mode of the methyl copper hydride anion, CH_3–CuH^-. The observed Cu–H stretching frequency and distinctively strong intensity are also reproduced by DFT computations (the B3LYP and BPW91 frequencies of 1606.1 and 1629.7 cm^{-1}) (Table S9†) for the singlet ground state anion. The triplet state is 212 kJ mol^{-1} higher in energy, and the strong Cu–H stretching mode predicted near 1470 cm^{-1} is not observed.

The CH_3–CuH, CH_3–Cu, and CH_3–CuH^- products are 85 kJ mol^{-1} higher, 203 kJ mol^{-1} lower, and 23 kJ mol^{-1} lower than the Cu(^{2}S) + CH_4, Cu(^{2}S) + CH_3, and Cu^-(^{1}S) + CH_4 reagents, respectively. Since the insertion reaction proceeds with Cu(^{2}P),[6a] which is 365 kJ mol^{-1} higher in energy than Cu(^{2}S),[27] CH_3–CuH is 279 kJ mol^{-1} lower in energy than Cu(^{2}P) + CH_4 reagents. The observed products are again the most stable among the corresponding plausible products. For example, the unidentified CH_2–CuH_2, CH_2–CuH, and CH_2–CuH_2^- are 158, 35, and 270 kJ mol^{-1} higher than the corresponding reagents.

Structures of small Au, Ag, and Cu complexes

The structures of the Group 11 metal complexes investigated in this study are illustrated in Fig. 7–9. The C–Au, C–Ag, and C–Cu bond lengths of the small Group 11 complexes are comparable to those of the previously introduced Au (1.9–2.3 Å),[29] Ag (2.1–2.5 Å),[30] and Cu (1.9–2.3 Å)[31] complexes, many of which are π-complexes. The computed C–Cu bond length of 1.918 Å for CH_3–Cu is slightly longer than that determined from the rotational spectrum (1.8841 Å).[5a] While CH_3–MH has a C_s structure, CH_3–M and CH_3–MH^- have C_{3v} structures.[8,32]

The CH_3–M molecules contain the shortest C–M bond, consistent with the high natural effective bond obtained from NBO analysis (Table S10†),[33] and the bonded C and M have mostly sp^3

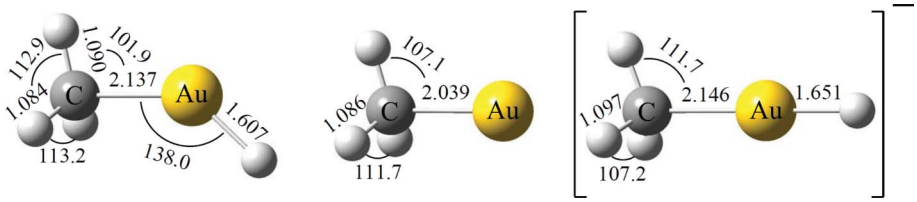

Fig. 7 The B3LYP structures of the identified Au products with the 6-311++G(3df,3pd) basis set for H, C, and Au. Bond distances and angles are in Å and deg. The methyl auride and anionic insertion complex (CH_3–Au and CH_3–AuH^-) have C_{3v} structures whereas the neutral insertion complex (CH_3–AuH) possesses a C_s structure.

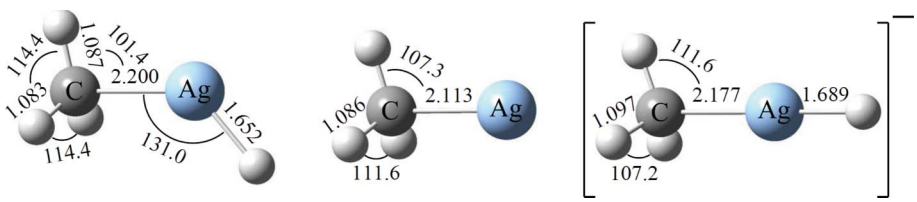

Fig. 8 The B3LYP structures of the Ag products with the 6-311++G(3df,3pd) basis set for H, C, and Ag. Bond distances and angles are in Å and deg. The methyl silver and anionic insertion complexes are identified in the matrix spectra (see text). The methyl silver and anionic insertion complex (CH_3–Ag and CH_3–AgH^-) have C_{3v} structures whereas the neutral insertion complex (CH_3–AgH) possesses a C_s structure.

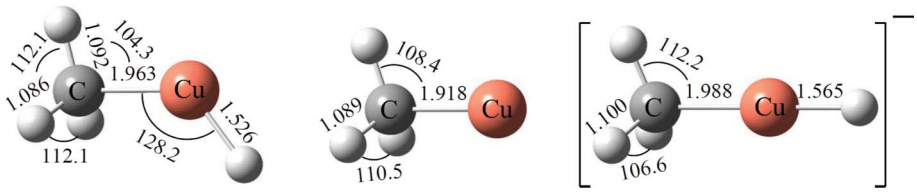

Fig. 9 The B3LYP structures of the identified Cu products with the 6-311++G(3df,3pd) basis set for H, C, and Cu. Bond distances and angles are in Å and deg. The methyl copper and anionic insertion complex (CH_3–Cu and CH_3–CuH^-) have C_{3v} structures whereas the neutral insertion complex (CH_3–CuH) possesses a C_s structure.

and sd hybridizations. For example, the C–Au bond in CH_3–Au consists of s(14.5%) and p(85.4%) for C and s(80.4%) and d(19.5%) for Au, indicating that the C–Au bond formation apparently does not require electron promotion from the electronic configuration of gold [Xe]$4f^{14}5d^{10}6s^1$. On the other hand, the slightly longer C–Au bonds of the insertion complexes CH_3–AuH and CH_3–AuH^- carry significant p contributions for Au. For example, Au has s(41.8%), p(24.1%), and d(34.0%) for the C–Au bond of CH_3–AuH and s(42.3%), p(47.0%), and d(10.4%) for that of CH_3–AuH^-.

Reactions

The reaction medium contains M atoms, CH_4, CH_3, and electrons, and thus, combinations of them can provide sources of the primary products (CH_3–MH, CH_3–M, and CH_3–MH^- from M + CH_4, M + CH_3, and M + e^- + CH_4, respectively). However, the concentrations of CH_3 and e^- in the reaction medium are low, and the alkyl metal and anionic insertion complexes have not been identified in the reactions of other transition-metal reactions while similar amounts of CH_3 and electrons are believed to exist in the matrix samples.[9–13] Therefore, generation of the methyl metal and anionic insertion complexes results from the unique properties of the coinage metals. The **i** absorptions in the original deposition spectra suggest that CH_3–MH is first produced *via* C–H insertion of CH_4 by M* (excited), similar to the previously studied transition-metal systems,[9–13] and the subsequent transformations to CH_3–M and CH_3–MH^- probably follow. The earlier copper–methane experiments demonstrated that ^{2}P excited Cu atoms were required for the reaction,[6a] and excitation in the laser ablation process and through subsequent UV irradiation provides this required energy.

$$M^*(^2P) + CH_4 \rightarrow CH_3\text{–}MH^* \rightarrow CH_3\text{–}MH \quad (1)$$

Release of H from CH_3–MH requires extra energy, which is consistent with the weak **a** absorptions in the original spectra. The excess energy from the insertion reaction or plume radiation would provide the energies for H-detachment from the Au, Ag, and Cu insertion complexes (134, 110 and 137 kJ mol^{-1}), generating the alkyl metal during co-deposition. The alkyl metals are relatively stable due to the single valence electrons (s^1) of the Group 11 metals,[34] leading to the much smaller H-detachment energies for the insertion complexes than those for other transition-metal analogues. For example, H-detachment energies of 290, 213, and 327 kJ mol^{-1} are estimated for CH_3–ZrH, CH_3–NiH and CH_3–PtH. In addition, the CH_3–M molecules can be prepared by direct combination reactions (2b) as the methyl radical is produced and trapped in these experiments from laser plume photodissociation of the methane precursor.

$$CH_3\text{–}MH^* \rightarrow CH_3\text{–}M + H \quad (2a)$$

$$CH_3 + M \rightarrow CH_3\text{–}M \quad (2b)$$

On the other hand, addition of an electron produced in the ablation process to the insertion complex is very exothermic. CH_3–AuH^- is 268 kJ mol^{-1} lower in energy than CH_3–AuH, which is in fact larger than the electron affinity of the Au atom, 223 kJ mol^{-1}.[1g,25] In parallel, electron attachments to CH_3–AgH and CH_3–CuH lower the energies by 252 and 226 kJ mol^{-1}, which are considerably larger than the electron affinities of the Ag and Cu atoms themselves, at 126 and 119 kJ mol^{-1}.[25] The higher electron affinities of the insertion complexes relative to those of the metal atoms are probably due to stabilization of negative charge by the methyl and hydride substituents: natural charges (Table S10†) on the methyl group ($3 \times 0.167 - 1.108 = -0.607$) and hydride (−0.413) for CH_3–AuH^- substantiate this rationale.

$$CH_3\text{–}MH + e^- \rightarrow CH_3\text{–}MH^- \quad (3)$$

The higher electron affinities of the insertion complexes also suggest that the insertion complex is probably formed first, and subsequent electron attachment produces the anionic insertion complex (CH_3–MH^-), which is observed here owing to the very high intensity of the metal–hydride vibration. This should be more efficient than the C–H insertion reaction by the electron-rich metal anion to form the product. The electron affinities of the coinage metal insertion complexes are also much higher than those of other transition-metal analogues, for example, 83, 165, and 94 kJ mol^{-1} for CH_3–ZrH, CH_3–NiH, and CH_3–PtH, and the electron affinities of Zr, Ni, and Pt are 41, 112, and 205 kJ mol^{-1}.[25] Finally, the corresponding methylene or methylidene complexes (CH_2–MH_2) are not observed probably due to their high energies.

Fig. 1–6 and S1–S3† also show that the $\mathbf{i}^-$ absorptions diminish upon UV and full arc irradiation while the **i** and **a** absorptions increase, suggesting that the anionic insertion complex photodetaches an electron to form the insertion and alkyl metal complexes during sample irradiation. The UV photon would provide CH_3–MH^- with the energy to detach an electron to generate the CH_3–MH and the excess reaction energy would in turn lead to dissociation of H to produce CH_3–M, reaction (4).

$$CH_3\text{–}MH^- + UV \rightarrow CH_3\text{–}MH^* + e^- \rightarrow CH_3\text{–}M + H + e^- \quad (4)$$

A 300 nm photon corresponds to 400 kJ mol^{-1}, which is roughly equal to the transformation energy from CH_3–AuH^- to CH_3–M *via* CH_3–MH; those for the Ag and Cu analogues are 361 and 278 kJ mol^{-1}.

The Au and Cu spectra also show that the **i** absorptions almost disappear on visible irradiation while the **a** band (and CuH

absorption in the Cu spectra), and the CH_3 absorption remain essentially unchanged, suggesting that a visible photon dissociates the insertion complex mostly to M + CH_4 in the matrix rather than to CH_3–M + H or CH_3 + MH.

Conclusions

Reactions of laser-ablated Group 11 metal atoms with methane isotopomers have been carried out, and the products are identified from the matrix IR spectra on the basis of frequencies, isotopic shifts, and correlation with two DFT frequency calculations. The insertion complexes (CH_3–MH) are identified along with methyl metal and anionic insertion complexes (CH_3–M, and CH_3–MH^-), showing that excited Group 11 metal atoms also readily undergo C–H insertion and subsequent reactions follow. The present results reconfirm that the C–H activation of alkanes by excited transition-metal atoms is a common phenomenon.[9–13] Facile hydride dissociation and high electron affinity of the coinage metal insertion complexes lead to generation of the unique methyl metal and anionic insertion products from the initially formed insertion complex.

DFT computations for the primary products reproduce not only the observed vibrational characteristics but their stabilities over other plausible products as well. The calculated C–M bond lengths for the Au, Ag, and Cu complexes are appropriate and in line with those of the previously investigated Group 11 metal complexes. The methyl metal species have the shortest computed C–M bond lengths, which are consistent with their highest effective bond orders, and the CH_3–MH complexes have higher electron affinities than the metal atoms. The NBO[33] analyses also show that in CH_3–MH and CH_3–MH^-, the metal atom has spd hybridization for the C–M bond, whereas in CH_3–M, the metal contributes mostly s character to the carbon–metal bond.

Acknowledgements

We gratefully acknowledge financial support from National Science Foundation (U. S.) Grant CHE 03-52487 to L. A., and support from the Korea Research Foundation (KRF) grant funded by the Korean government (MEST) (No 2010-0016527).

References

1 (*a*) H. Schmidbaur and A. Schier, *Organometallics*, 2010, **29**, 2; (*b*) B. Armer and H. Schmidbaur, *Angew. Chem., Int. Ed. Engl.*, 1970, **9**, 101; (*c*) D. J. Gorin, B. D. Sherry and F. D. Toste, *Chem. Rev.*, 2008, **108**, 3351; (*d*) A. Arcadi, *Chem. Rev.*, 2008, **108**, 3266; (*e*) E. Jiménez-Núñez and A. M. Echavarren, *Chem. Rev.*, 2008, **108**, 3326; (*f*) Z. Li, C. Brouwer and C. He, *Chem. Rev.*, 2008, **108**, 3239; (*g*) P. Pyykko, *Angew. Chem., Int. Ed.*, 2004, **43**, 4412. (Au reviews).
2 (*a*) J.-M. Weibel, A. Blanc and P. Pale, *Chem. Rev.*, 2008, **108**, 3149; (*b*) W. Tyrra, *Heteroat. Chem.*, 2002, **13**, 561. (Ag reviews).
3 (*a*) B. Breit and Y. Schmidt, *Chem. Rev.*, 2008, **108**, 2928; (*b*) V. Caprio, *Lett. Org. Chem.*, 2006, **3**, 339. (Cu reviews).
4 (*a*) R. A. J. O'Hair, *Chem. Commun.*, 2002, 20; (*b*) B. S. Rabinovitch, D. H. Dills and N. R. Larson, *J. Phys. Chem.*, 1959, **63**, 1523; (*c*) G. Semerano and L. Riccoboni, *Ber. Dtsch. Chem. Ges. B*, 1941, **74**, 1089. (CH_3–Ag).
5 (*a*) D. B. Grotjahn, D. T. Halfen, L. M. Ziurys and A. L. Cooksy, *J. Am. Chem. Soc.*, 2004, **126**, 12621; (*b*) E. Nakamura, S. Mori, M. Nakamura and K. Morokuma, *J. Am. Chem. Soc.*, 1997, **119**, 4887; (*c*) H. Gilman, R. G. Jones and L. A. Woods, *J. Org. Chem.*, 1952, **17**, 1630. (CH_3–Cu).
6 (*a*) J. M. Parnis, S. A. Mitchell, J. Garcia-Prieto and G. A. Ozin, *J. Am. Chem. Soc.*, 1985, **107**, 8169; see also; (*b*) W. E. Billups, M. M. Konarski, R. H. Hauge and J. L. Margrave, *J. Am. Chem. Soc.*, 1980, **102**, 7393; (*c*) D. Ritter, J. J. Carroll and J. C. Weisshaar, *J. Phys. Chem.*, 1992, **96**, 10636.
7 S.-C. Chang, Z. H. Kafafi, R. H. Hauge, W. E. Billups and J. L. Margrave, *J. Am. Chem. Soc.*, 1987, **109**, 4508.
8 (*a*) N. J. Rijs and R. A. J. O'Hair, *Organometallics*, 2010, **29**, 2282; (*b*) N. J. Rijs and R. A. O'Hair, *Organometallics*, 2009, **28**, 2684. (CH_3–AgH^- and CH_3–CuH^-).
9 L. Andrews and H.-G. Cho, *Organometallics*, 2006, **25**, 4040, and references therein (review article, Groups 4–6).
10 (*a*) H.-G. Cho and L. Andrews, *Organometallics*, 2007, **26**, 633; (*b*) H.-G. Cho and L. Andrews, *J. Phys. Chem. A*, 2008, **112**, 1519; (*c*) H.-G. Cho and L. Andrews, *J. Phys. Chem. A*, 2006, **110**, 3886. (Groups 3, 4 and 5).
11 (*a*) H.-G. Cho and L. Andrews, *Inorg. Chem.*, 2008, **47**, 1653; (*b*) H.-G. Cho and L. Andrews, *Organometallics*, 2007, **26**, 4098; (*c*) H.-G. Cho and L. Andrews, *Organometallics*, 2008, **27**, 1786. (Re and Os).
12 (*a*) H.-G. Cho and L. Andrews, *J. Phys. Chem. A*, 2008, **112**, 12293; (*b*) H.-G. Cho and L. Andrews, *Organometallics*, 2009, **28**, 1358. (Pt).
13 (*a*) L. Andrews and H.-G. Cho, *J. Phys. Chem. A*, 2005, **109**, 6796; (*b*) J. T. Lyon, L. Andrews, P.-Å Malmqvist, B. O. Roos, T. Yang and B. E. Bursten, *Inorg. Chem.*, 2007, **46**, 4917. (actinides); (*c*) H.-G. Cho, L. Andrews, unpublished work (lanthanides).
14 (*a*) G. von Frantzius, R. Streubel, K. Brandhorst and J. Grunenberg, *Organometallics*, 2006, **25**, 118, and references therein; (*b*) N. Berkaine, P. Reinhardt and M. E. Alikhani, *Chem. Phys.*, 2008, **343**, 241; (*c*) G. Chung and M. S. Gordon, *Organometallics*, 2003, **22**, 42; (*d*) G. T. de Jong and F. M. Bickelhaupt, *J. Chem. Theory Comput.*, 2007, **3**, 514; (*e*) B. O. Roos, R. Lindh, H.-G. Cho and L. Andrews, *J. Phys. Chem. A*, 2007, **111**, 6420.
15 (*a*) L. Andrews and A. Citra, *Chem. Rev.*, 2002, **102**, 885, and references therein; (*b*) L. Andrews, *Chem. Soc. Rev.*, 2004, **33**, 123, and references therein.
16 M. J. Frisch, G. W. Trucks, H. B. Schlegel, G. E. Scuseria, M. A. Robb, J. R. Cheeseman, J. A. Montgomery, Jr., T. Vreven, K. N. Kudin, J. C. Burant, J. M. Millam, S. S. Iyengar, J. Tomasi, V. Barone, B. Mennucci, M. Cossi, G. Scalmani, N. Rega, G. A. Petersson, H. Nakatsuji, M. Hada, M. Ehara, K. Toyota, R. Fukuda, J. Hasegawa, M. Ishida, T. Nakajima, Y. Honda, O. Kitao, H. Nakai, M. Klene, X. Li, J. E. Knox, H. P. Hratchian, J. B. Cross, V. Bakken, C. Adamo, J. Jaramillo, R. Gomperts, R. E. Stratmann, O. Yazyev, A. J. Austin, R. Cammi, C. Pomelli, J. Ochterski, P. Y. Ayala, K. Morokuma, G. A. Voth, P. Salvador, J. J. Dannenberg, V. G. Zakrzewski, S. Dapprich, A. D. Daniels, M. C. Strain, O. Farkas, D. K. Malick, A. D. Rabuck, K. Raghavachari, J. B. Foresman, J. V. Ortiz, Q. Cui, A. G. Baboul, S. Clifford, J. Cioslowski, B. B. Stefanov, G. Liu, A. Liashenko, P. Piskorz, I. Komaromi, R. L. Martin, D. J. Fox, T. Keith, M. A. Al-Laham, C. Y. Peng, A. Nanayakkara, M. Challacombe, P. M. W. Gill, B. G. Johnson, W. Chen, M. W. Wong, C. Gonzalez and J. A. Pople, *GAUSSIAN 03 (Revision C.02)*, Gaussian, Inc., Wallingford, CT, 2004.
17 (*a*) A. D. Becke, *J. Chem. Phys.*, 1993, **98**, 5648; (*b*) C. Lee, Y. Yang and R. G. Parr, *Phys. Rev. B*, 1988, **37**, 785.
18 K. Raghavachari and G. W. Trucks, *J. Chem. Phys.*, 1989, **91**, 1062.
19 D. Andrae, U. Haeussermann, M. Dolg, H. Stoll and H. Preuss, *Theor. Chim. Acta*, 1990, **77**, 123.
20 (*a*) A. D. Becke, *Phys. Rev. A: At., Mol., Opt. Phys.*, 1988, **38**, 3098; (*b*) K. Burke, J. P. Perdew, Y. Wang, in *Electronic Density Functional Theory: Recent Progress and New Directions*, ed. J. F. Dobson, G. Vignale, M. P. Das, Plenum, 1998.
21 M. Head-Gordon and T. Head-Gordon, *Chem. Phys. Lett.*, 1994, **220**, 122.
22 A. P. Scott and L. Radom, *J. Phys. Chem.*, 1996, **100**, 16502.
23 M. P. Andersson and P. L. Uvdal, *J. Phys. Chem. A*, 2005, **109**, 2937.
24 (*a*) L. Andrews and X. Wang, *J. Am. Chem. Soc.*, 2003, **125**, 11751; (*b*) X. Wang, L. Andrews, L. Manceron and C. Marsden, *J. Phys. Chem. A*, 2003, **107**, 8492. (Au, Ag, Cu + H_2).
25 http://en.wikipedia.org/wiki/Electron_affinity.
26 P. Schwerdtfeger, P. D. W. Boyd, A. K. Burrell, W. T. Robinson and M. J. Taylor, *Inorg. Chem.*, 1990, **29**, 3593.
27 C. E. Moore, *Atomic energy levels as derived from the analyses of optical spectra (Circular 467 of the US National Bureau of Standards)*, National Bureau of Standards, Washington DC, 1958.

28 D. E. Milligan and M. Jacox, *J. Chem. Phys.*, 1967, **47**, 5146. (CH_3).
29 (*a*) K. Köhler, S. J. Silverio, I. Hyla-Kryspin, R. Gleiter, L. Zsolnai, A. Driess, G. Huttner and H. Lang, *Organometallics*, 1997, **16**, 4970; (*b*) M. Pažický, A. Loos, M. J. Ferreira, D. Serra, N. Vinokurov, F. Rominger, C. Jäkel, A. S. K. Hashmi and M. Limbach, *Organometallics*, 2010, **29**, 4448. (Au complexes).
30 (*a*) J. C. Barrick, D. C. Canfield and B. C. Giessen, *Acta Crystallogr., Sect. B: Struct. Crystallogr. Cryst. Chem.*, 1979, **35**, 464; (*b*) B. Gil, J. Forniés, J. Gómez, E. Lalinde, A. Martin and M. T. Moreno, *Inorg. Chem.*, 2006, **45**, 7788. (C–Ag bond length).
31 (*a*) M. D. Janssen, K. Köhler, M. Herres, A. Dedieu, W. J. J. Smeets, A. L. Spek, D. M. Grove, H. Lang and G. V. Koten, *J. Am. Chem. Soc.*, 1996, **118**, 4817; (*b*) B. J. Bellott and G. S. Girolami, *Organometallics*, 2009, **28**, 2046. (C–Cu bond length).
32 (*a*) I. Antes and G. Frenking, *Organometallics*, 1995, **14**, 4263; (*b*) W. Nakanishi, M. Yamanaka and E. Nakamura, *J. Am. Chem. Soc.*, 2005, **127**, 1446. (CH_3–M structures).
33 A. E. Reed, L. A. Curtiss and F. Weinhold, *Chem. Rev.*, 1988, **88**, 899, and references therein.
34 http://www.webelements.com.

